Femtosecond Fluorescence Dynamics of Porphyrin in Solution and Solid Films: The Effects of Aggregation and Interfacial Electron Transfer between Porphyrin and TiO$_2$

Liyang Luo,[†] Chen-Fu Lo,[‡] Ching-Yao Lin,*[,‡] I-Jy Chang,[§] and Eric Wei-Guang Diau*[,†]

Department of Applied Chemistry, Institute for Molecular Science and Center for Interdisciplinary Molecular Science, National Chiao Tung University, Hsinchu, Taiwan 300, Department of Applied Chemistry, National Chi Nan University, Puli, Nantou Hsien, Taiwan 545, and Department of Chemistry, National Taiwan Normal University, Taipei, Taiwan 116

The excited-state relaxation dynamics of a synthetic porphyrin, ZnCAPEBPP, in solution, coated on a glass substrate as solid films, mixed with PMMA and coated on a glass substrate as solid films, and sensitized on nanocrystalline TiO$_2$ films were investigated by using femtosecond fluorescence up-conversion spectroscopy with excitation in the Soret band, S$_2$. We found that the S$_2 \rightarrow$ S$_1$ electronic relaxation of ZnCAPEBPP in solution and on PMMA films occurs in 910 and 690 fs, respectively, but it becomes extremely rapid, <100 fs, in solid films and TiO$_2$ films due to formation of porphyrin aggregates. When probed in the S$_1$ state of porphyrin, the fluorescence transients of the solid films show a biphasic kinetic feature with the rapid and slow components decaying in 1.9−2.4 and 19−26 ps, respectively. The transients in ZnCAPEBPP/TiO$_2$ films also feature two relaxation processes but they occur on different time scales, 100−300 fs and 0.8−4.1 ps, and contain a small offset. According to the variation of relaxation period as a function of molecular density on a TiO$_2$ surface, we assigned the femtosecond component of the TiO$_2$ films as due to indirect interfacial electron transfer through a phenylethynyl bridge attached to one of four meso positions of the porphyrin ring, and the picosecond component arising from intermolecular energy transfer among porphyrins. The observed variation of aggregate-induced relaxation periods between solid and TiO$_2$ films is due mainly to aggregation of two types: J-type aggregation is dominant in the former case whereas H-type aggregation prevails in the latter case.

1. Introduction

The most efficient dye-sensitized solar cells (DSC) with use of ruthenium polypyridyl complexes as photosensitizers and nanocrystalline TiO$_2$ films as semiconductor substrates have achieved energy conversion efficiency greater than 10%.[1−3] In addition to the enhanced surface area due to the nanoporous nature of TiO$_2$ films, which greatly increases the light-harvesting capability,[1a] there are two interfacial electron-transfer (IET) processes, forward and backward IET, believed to be critical to the overall efficiency of a DSC.[1b] The forward IET ensures electron injection from the electronically excited state of the molecular dyes into the conduction band of TiO$_2$ through the carboxylate group that transports electrons effectively.[2] The electrons injected into the conduction band might recombine with the dye cation through the backward IET channel, thus reducing the dye molecule to the ground state.[1,2] Understanding the mechanistic features and the corresponding dynamics of these IET processes would help to improve further the efficiency of the photovoltaic effect in solar energy conversion and storage.

The electron-injection dynamics of dye/TiO$_2$ systems based on femtosecond (fs) transient absorption measurements were first reported from the pioneering work of Tachibana et al.;[4] they observed a biphasic temporal profile of which the rapid component decays in <150 fs and the slow one in 1.2 ps. Later, Lian and co-workers[5] employed fs transient IR spectroscopy to study the IET dynamics of dye-sensitized nanocrystalline TiO$_2$ thin-film systems; their research focused mainly on Grätzel's N3/TiO$_2$ system, and several analogous dye-semiconductor systems were also investigated.[5d,6] These authors found that the forward IET process was characterized by an ultrarapid component with a time constant smaller than 100 fs, and a slow component that is sensitive to sample conditions. Furthermore, the rate of electron injection from the N3 dye to various semiconductors obeyed a trend TiO$_2$ > SnO$_2$ > ZnO, indicating a strong dependence on the nature of the semiconductor; the rate of injection depended on the redox potential of the photosensitizer, pH of the solution, and excitation energy. A two-state injection model was proposed: the rapid, <100 fs, component was attributed to injection from a nonthermalized excited state and the slow component to injection from the thermalized excited state of the dye.

Sundström and co-workers discussed the issue of forward IET rates for N3/TiO$_2$ and other related systems based on measurements of fs UV/visible transient absorption spectra.[7] Their results are similar to those of others who found the interfacial dynamical process of the N3/TiO$_2$ family to involve two distinct time scales. The assignment made by the former group is also similar: the sub-100-fs component corresponds to electron injection from the singlet excited state, [1]MLCT, of a sensitizer to the conducting band of TiO$_2$ nanoparticles, whereas the 1−10-ps component relates to electron injection from the triplet excited state, [3]MLCT, to the conducting band of the TiO$_2$ nanoparticles.

---

* Address correspondence to this author. Fax: (886)-03-572-3764. E-mail: diau@mail.ac.nctu.edu.tw.
† National Chiao Tung University.
‡ National Chi Nan University.
§ National Taiwan Normal University.

Femtosecond Fluorescence Dynamics of Porphyrin

J. Phys. Chem. B, Vol. 110, No. 1, 2006 **411**

The work of Kuciauskas et al.[8] using ruthenium and osmium polypyridyl complexes as photosensitizers supported his two-state mechanism. Furthermore, because the excited state is localized on a ligand of the sensitizer that is not attached to the semiconductor, the rate of so-called "interligand" electron transfer was found also to occur on a ps time scale.[7e] Kallioninen et al.[7f] compared all recent temporally resolved experiments under varied conditions of sample preparation and concluded that a large photon energy of the pump and exposure of the sensitized film to air considerably altered the slower (ps) kinetics; these effects were attributed mostly to degradation of the dye. In addition, the observed nonstatistical behavior of electron injection implies that interfacial electron injection might occur from a photosensitizer with an excited-state redox potential below the conduction band edge of the semiconductor, indicating that the forward IET following an "upstream" potential-energy pathway is possible.[7a]

Ultrarapid IET dynamics of many other systems with use of organic dyes as photosensitizers have been investigated.[9−17] A common feature of the forward IET dynamics of all dye/TiO$_2$ systems is the biphasic nature of decay of the transients with rapid and slow processes occurring on fs and ps time scales, respectively; the rapid process has been coherently assigned to involve electron injection directly from dye to TiO$_2$ whereas the assignment of the slow process remains under discussion. For example, Wenger et al.[18] reported that the slow component of the N3/TiO$_2$ system is due to the aggregated state of the dye, which is against the two-state mechanism aforementioned. Another ultrarapid investigation[19] indicates, however, that the electron-injection dynamics of the porphyrin/TiO$_2$ system are similar to those of the N3/TiO$_2$ system, making the former system a prospective candidate for DSC applications.[20−24]

The capability of porphyrins to absorb visible light in the 400−450 nm region (B or Soret band) and in the 500−700 nm region (Q bands) has been used in the design of artificial light-harvesting systems.[25] As examples, multiporphyrin arrays have been constructed with several linkers that are suitable for the preparation of linear or extended architectures via attachment at the meso position.[26,27] Recent advances in organic synthesis have allowed the preparation of linear and semirigid harvesting arrays with use of porphyrin pigments linked by phenylethyne (PE) spacers.[28] On the basis of a similar idea, we have designed zinc porphyrin pigments to serve as photosensitizers in our investigation of interfacial electron-transfer dynamics between porphyrins and TiO$_2$ in a systematic way. The molecular structure of the sensitizer system is comprised of three parts: a zinc biphenylporphyrin (ZnBPP) unit serves as light-harvesting center to provide photoinduced electrons, the PE group is connected to the meso position of the porphyrin to transfer the electrons efficiently, and the carboxylic acid (CA) attached to the end of the spacer serves as an anchoring group to bond tightly onto the surface of TiO$_2$ nanoparticles. To vary systematically the distance between the electron donor (porphyrin) and the electron acceptor (TiO$_2$), the π-conjugated linker has been extended from one to four PE spacers with only one CA end group; hence we denote the porphyrin pigments as ZnCA-(PE)$_x$BPP, with $x = 1−4$ for the series; the chemical structure of ZnCAPEBPP is shown in Chart 1.

Most recent results on IET dynamics of dye/semiconductor systems were obtained from fs transient absorption measurements, but there are few reports on such systems based on using the fs fluorescence decay methods (e.g., ref 9) because of the minuscule quantum yield of fluorescence in the presence of the IET process. Fluorescence decay methods offer, however, a

CHART 1: Chemical Structure of ZnCAPEBPP
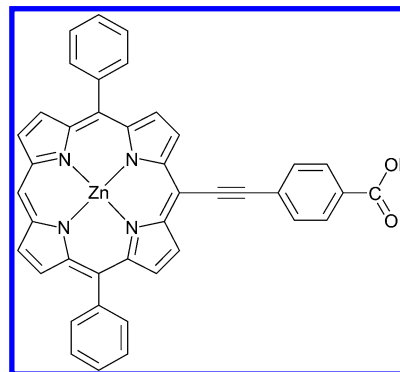
unique detection window to monitor only the relaxation process occurring in the excited state of the dye without involving the complicated ionic states of the dye and the semiconductor after charge separation. Thus, interpretation of kinetic data obtained from these fluorescence decay methods should be simpler and more straightforward than that obtained from transient absorption methods. In the present work, we have employed a fs fluorescence up-conversion technique to interrogate the forward IET dynamics of the ZnCAPEBPP-sensitized TiO$_2$ nanocrystalline films upon excitation into the S$_2$ state of the porphyrin ($\lambda_{ex} = 420−430$ nm). Because aggregation of porphyrins might be a drawback for photoenergy conversion, we have assessed the effect of aggregation through comparison of the relaxation dynamics obtained from ZnCAPEBPP/THF solution, pure ZnCAPEBPP deposited on a plate-glass substrate, and the ZnCAPEBPP/PMMA mixture deposited on a plate-glass substrate. We found that S$_2$ → S$_1$ internal conversion (IC) of ZnCAPEBPP becomes extremely rapid when the porphyrin molecules stack together to form J-type aggregates; the S$_1$ species are produced within that time scale, <100 fs, but disappear with a biphasic dynamical nature: the rapid component decays in ∼2 ps whereas the slow one decays in ∼20 ps. The fluorescence transients of the ZnCAPEBPP/TiO$_2$ system observed in the S$_1$ state also feature two major decay components, but the decay coefficients are on much shorter time scales: 100−300 fs and 1−4 ps for the rapid and slow decays, respectively. We assigned the rapid component to electron injection from porphyrin to TiO$_2$; the slow component, of which the decay coefficients are sensitive to the molecular density of porphyrins on TiO$_2$ films, are due mainly to intermolecular energy transfer among porphyrins.

2. Experimental Section

2.1. Materials. A standard Sonogashira cross-coupling method was used to synthesize porphyrin ZnCAPEBPP.[29] The reactions were monitored by TLC and UV/visible spectra. Cross-coupling mono-brominated biphenylporphinato zinc with 3 equiv of 4-ethynylbenzoic acid typically afforded ZnCAPEBPP in 80% yield after purification on silica gel with MeOH/CH$_2$Cl$_2$ eluants and crystallization from THF/hexane. 4-Ethynylbenzoic acid was prepared from trimethylsilylethyne and 4-iodobenzoic acid in 65% yield. A glovebox (MBraun Uni-lab), a vacuum line, and standard Schlenk techniques were employed to process all materials sensitive to air. Solvents (Merck, Darmstadt, Germany), Pd(PPh$_3$)$_4$ catalyst (Strem Chemical Inc, MA), and other chemicals (Acros Organics, NJ) were obtained from the indicated suppliers. Solvents used in cross-coupling experiments were purified according to literature methods.[30] Chromatographic purification was performed with silica gel 60 (230−
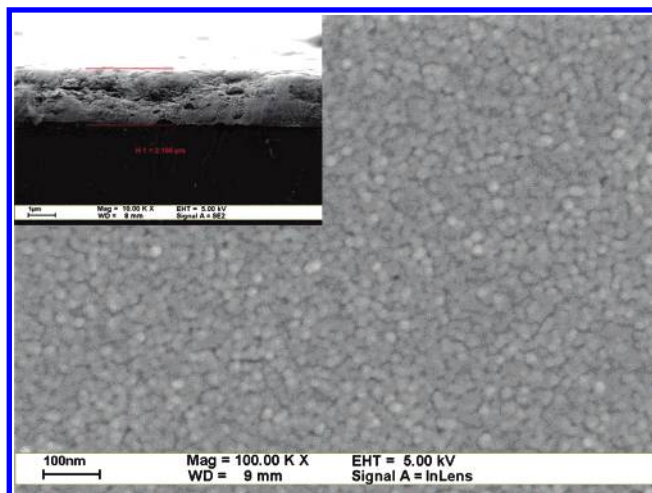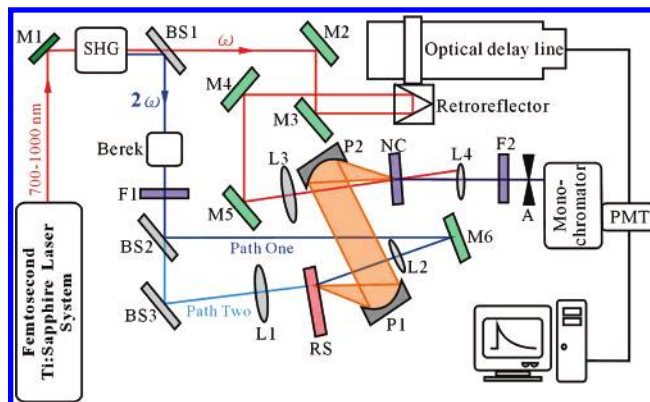
Figure 1. SEM photomicrographs of an unsensitized TiO_2 film. The average size of particles is ∼15 nm; the thickness of the film is ∼2 μm.

Figure 2. Femtosecond fluorescence up-conversion spectrometer setup: A, aperture or iris; BS1−BS3, beam splitters; F1−F2, color filters; L1−L4, focusing lenses; M1−M6, broadband dielectric mirrors; NC, nonlinear crystal; P1−P2, parabolic mirrors; RS, rotary sample cell; PMT, photomultiplier tube; SHG, optical set for second harmonic generation.

400 mesh, Merck). All NMR solvents (Cambridge Isotope Lab, Inc.) were used as received. Data for characterization of ZnCAPEBPP follow: ^{1}H NMR (d_6-DMSO at 2.50 ppm) 10.36 (s, 1H), 9.84 (d, $J = 5$ Hz, 2H), 9.46 (d, $J = 5$ Hz, 2H), 8.92 (d, $J = 5$ Hz, 2H), 8.84 (d, $J = 5$ Hz, 2H), 8.25 (m, 8H), 7.86 (m, 6H). Elemental analysis of $C_{41}H_{24}N_4O_2Zn \cdot THF$, calculated C 72.83, H 4.35, N 7.55, found C 72.35, H 4.60, N 7.27.

2.2. Sample Preparation. Samples were prepared in both solution and thin films. For solutions, ZnCAPEBPP was dissolved in THF (Merck, spectral grade) to form a homogeneous solution of concentration 1.0×10^{-5} M. The pure ZnCAPEBPP solid films were obtained by spin-coating the ZnCAPEBPP/THF solution onto a plate-glass substrate and allowing the solvent to evaporate slowly in a vacuum hood. To make thin films in solid solution, we mixed ZnCAPEBPP with a transparent polymer, poly(methyl methacrylate) (PMMA), in a 1:5000 ratio by mass. The ZnCAPEBPP/PMMA mixture was dissolved in trichloromethane (Merck, pro analysi) to form a viscous solution and then smoothly deposited onto a glass plate via a standard spin-coating procedure.

The procedure for synthesis of TiO_2 nanoparticles is described elsewhere.[31] Briefly, a quantity of titanium isopropoxide was added, dropwise at 25 °C, to nitric acid (0.1 M, 750 mL) under vigorous stirring. Immediately after this hydrolysis, the white slurry was heated at 80 °C and the solution was stirred vigorously for 8 h to achieve peptization. The nanoparticle thin films of TiO_2 were prepared with 15 layers by spin-coating on glass and heating at 450 °C in an oven for 30 min. The electron micrograph of the TiO_2 nanocrystalline thin film (Figure 1) shows that the size of TiO_2 particles is about 15 nm and the film thickness is ∼2 μm. Porphyrin molecules were adsorbed onto TiO_2 nanocrystalline thin films from ZnCAPEBPP solutions in THF/CH_2Cl_2 (1:14) for 4 h. To examine the effect of aggregation affecting the observed IET dynamics, we prepared three porphyrin-sensitized TiO_2 thin-film samples with initial concentrations 37 (Film 1), 73 (Film 2), and 150 μM (Film 3) of porphyrin solutions.

2.3. Steady-State Spectral Measurements. UV/visible absorption spectra of ZnCAPEBPP in solution and in solid thin films were recorded with a standard spectrophotometer (Cary 50, Varian). Emission spectra were measured with a composite CCD spectrometer (USB2000FLG, Ocean Optics) via a Y-shape fiber (R600-UV, Ocean Optics) for front-face probes. The excitation source contains a pulsed diode-laser head (LDH-P-

C-440, PicoQuant) coupled with a laser-diode driver (PDL-800B, PicoQuant) that produces excitation pulses at 435 nm with an average power of ∼300 μW.

2.4. Time-Resolved Fluorescence Measurements. Figure 2 shows the experimental setup for femtosecond (fs) time-resolved fluorescence measurements. Basically, a fluorescence optically gated (up-conversion) system (FOG100, CDP) is implemented in combination with a mode-locked Ti-sapphire laser (Mira 900D, Coherent) pumped with a 10-W Nd:YVO4 laser (Verdi-V10, Coherent). The femtosecond laser system generates output pulses at 860 nm (or 840 nm) with duration ∼120 fs at a repetition rate of 76 MHz. The frequency of the laser pulse was doubled for excitation ($\lambda_{ex} = 430$ or 420 nm). The residual fundamental pulse was used as an optical gate; a dichroic beam splitter served to separate excitation and gate beams. The excitation beam intensity was appropriately attenuated, and then focused onto a 1-mm rotating cell containing either the solution or the solid thin-film samples. The fs system includes two optical paths for excitation: path one is designed for measurements of thin-film samples via collection of emission from the front face; path two is designed for measurements of solution samples via collection of emission from the back face.[32] The emission was collected with two parabolic mirrors and focused onto a crystal (BBO type-I); the gate pulse was also focused on that BBO crystal for sum-frequency generation. The latter signal was collected with a lens, and separated from interference light with an iris, a band-pass filter, and a double monochromator (DH10, Jobin Yvon) in combination, then detected with a photomultiplier (R1527P, Hamamatsu) connected to a computer-controlled photon-counting system. On varying the temporal delay between gate and excitation pulses via a stepping-motor translational stage, we obtained a temporal profile (transient). The polarization between pump and probe pulses was fixed at the magic-angle condition, 54.7°.

2.5. Data Analysis and Kinetic Model. The fluorescence transient signal, $I(t)$, was fitted through convolution of the instrument-response function $g(t)$ with an appropriate molecular-response function $f(t)$,[33,34]

$$I(t) = \int_0^\infty g(t - s)f(s) \, ds \tag{1}$$

in which $g(t)$ is a Gaussian function; the choice of $f(t)$ relies on a proper kinetic model. When a rising feature appears in the transients, a consecutive kinetic model is employed to fit

Femtosecond Fluorescence Dynamics of Porphyrin

J. Phys. Chem. B, Vol. 110, No. 1, 2006 **413**
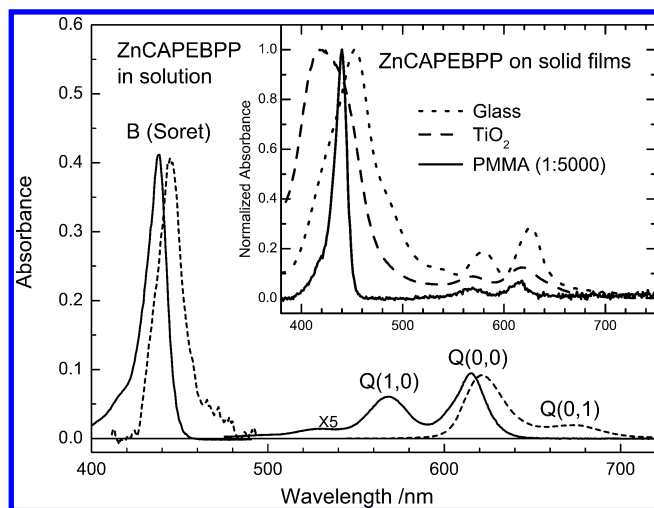
Figure 3. Absorption (solid curves) and fluorescence (dashed curves) spectra of ZnCAPEBPP in THF with B (Soret) and Q bands (enlarged by a factor 5) as indicated. The sample concentration was 5×10^{-6} M. The inset shows relative absorption spectra of ZnCAPEBPP deposited as a pure film on a glass substrate (dotted curve) mixed with PMMA (1:5000) to form a uniform thin film on a glass substrate (solid curve) and sensitized on a nanocrystalline TiO$_2$ thin film (dashed curve). The absorbance of each spectrum in the inset is normalized at the maximum of the S$_2$ band for comparison.

appropriately the transients,

$$A \overset{\tau_1}{\longrightarrow} B \overset{\tau_2}{\longrightarrow} C \qquad (2)$$

in which component A is described with a single-exponential function with a decay coefficient τ_1 and component B is described with a biexponential function with a rise coefficient τ_1 and a decay coefficient τ_2. The molecular response function $f(t)$ is expressed accordingly as

$$f(t) = a \exp\left(-\frac{t}{\tau_1}\right) + b\left[\exp\left(-\frac{t}{\tau_2}\right) - \exp\left(-\frac{t}{\tau_1}\right)\right] \qquad (3)$$

in which the preexponential factors a and b represent the relative weights (or amplitudes) of components A and B, respectively. Alternatively, a parallel kinetic model is employed to account for the observed temporal profiles showing a biphasic dynamical feature

$$A \overset{\tau_1}{\longrightarrow} B \qquad (4)$$

$$A' \overset{\tau_2}{\longrightarrow} B' \qquad (5)$$
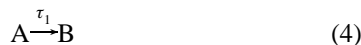
in which components A and A′ are described with a single-exponential function and decay coefficients τ_1 and τ_2, respectively. The molecular response function $f(t)$ is expressed accordingly as

$$f(t) = a \exp\left(-\frac{t}{\tau_1}\right) + b \exp\left(-\frac{t}{\tau_2}\right) \qquad (6)$$

in which the preexponential factors a and b represent the relative weights (or amplitudes) of components A and A′, respectively.

3. Results and Discussion

3.1. Steady-State Spectra of ZnCAPEBPP in Various Environments. Figure 3 shows the UV/visible absorption (solid curves) and fluorescence (dashed curves) spectra of Zn-CAPEBPP in THF solution; the inset shows the normalized

absorption spectra of ZnCAPEBPP on solid films of various types. The absorption spectrum in solution consists of two branches, the B (or Soret) band and the Q bands, traditionally identified as the S$_2$ ← S$_0$ and S$_1$ ← S$_0$ transitions, respectively. Maxima of these bands at 435, 560, and 615 nm are assigned as B(0,0), Q(1,0), and Q(0,0), respectively; the number of quanta shown in parentheses represents the dominant Franck−Condon active vibrational mode. The fluorescence spectrum in solution (dashed curves) clearly shows both S$_2$ → S$_0$ and S$_1$ → S$_0$ emissions with the corresponding maxima located at 447 and 621 (and 670) nm, respectively.

Because of aggregation, the sharp Soret band in solution becomes substantially broadened when porphyrin molecules are coated on a plate-glass substrate as a thin film or on a TiO$_2$-nanocrystalline thin film, shown as a dotted curve or dashed curve in the inset of Figure 3, respectively. Furthermore, the absorption maxima of the molecule on a glass film are red-shifted with respect to those in solution, indicating that the head-to-tail (J-type) aggregation might be involved upon formation of porphyrin aggregates in films. In contrast, the Soret band of the TiO$_2$ film is shifted toward the blue side of the spectrum, indicating that formation of porphyrin aggregates inside the nanoenvironment of a TiO$_2$ thin film is mainly of H type. When the porphyrin molecules were evenly distributed within a PMMA matrix, the aggregation effect was minimized and the absorption spectrum of a PMMA film (solid curve shown in the inset of Figure 3) is identical with that of solution. To improve our understanding of the effects of aggregation and interfacial energy transfer between porphyrins and TiO$_2$ nano-particles, we performed a time-resolved investigation on Zn-CAPEBPP in the above environments using a femtosecond fluorescence up-conversion method.

3.2. Relaxation Dynamics of ZnCAPEBPP in Solution. Porphyrin molecules behave as if effectively separate in THF solvent.[35] Therefore, time-resolved spectral data in ZnCAPEBPP/THF solution provide pertinent information about the dynamical behavior of porphyrin monomers in free solvents. Figure 4A shows three fluorescence transients of a ZnCAPEBPP/THF solution with excitation at $\lambda_{ex} = 420$ nm and emission observed at $\lambda_{em} = 470$, 620, and 675 nm. The transient at $\lambda_{em} = 470$ nm (circles) is well fitted with a single-exponential decay function with a decay coefficient $\tau = 910 \pm 10$ fs; the uncertainty represents two standard errors. The transients observed at $\lambda_{em} = 620$ (squares) and 675 nm (triangles) differ remarkably from the transient observed at $\lambda_{em} = 470$ nm: the former show a rising feature with a rise coefficient comparable to the decay coefficient of the latter in the short-time region; the transient signals of the former increase gradually to an asymptotic level in the long-time region, as shown in parts B and C of Figure 4 for $\lambda_{em} = 620$ and 675 nm, respectively. According to the steady-state spectral measurements shown in Figure 3, the transients observed at $\lambda_{em} = 470$ and 620 nm (and 675 nm) reflect the dynamical behavior occurring in the S$_2$ and S$_1$ electronic states, respectively. We therefore conclude that the S$_2$ → S$_1$ internal conversion of ZnCAPEBPP in solution takes ∼1 ps and the vibrationally hot S$_1$ species are produced on that time scale.

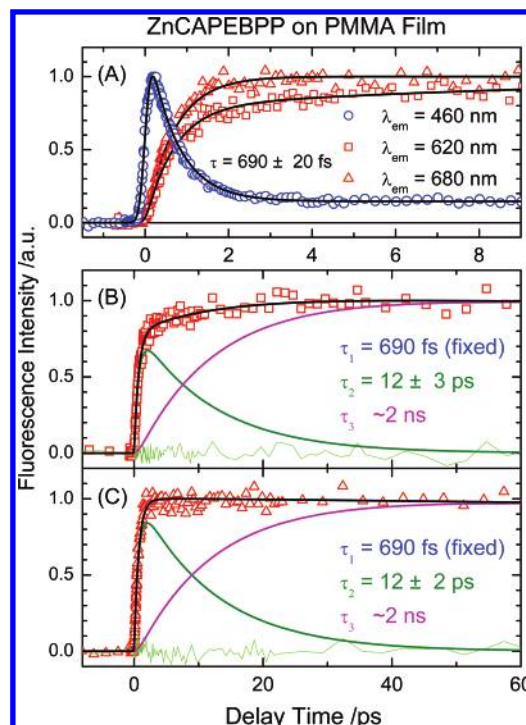Because of the rising character of the transients shown in Figure 4, the transients observed at $\lambda_{em} = 620$ and 675 nm are described satisfactorily according to a consecutive kinetic model with two components convoluted with the laser pulse: the first component (olive curves) rises in $\tau_1 = 910$ fs and then decays in $\tau_2 \sim 9$ ps whereas the second component (magenta curves) appears following the decay of the first component but persists
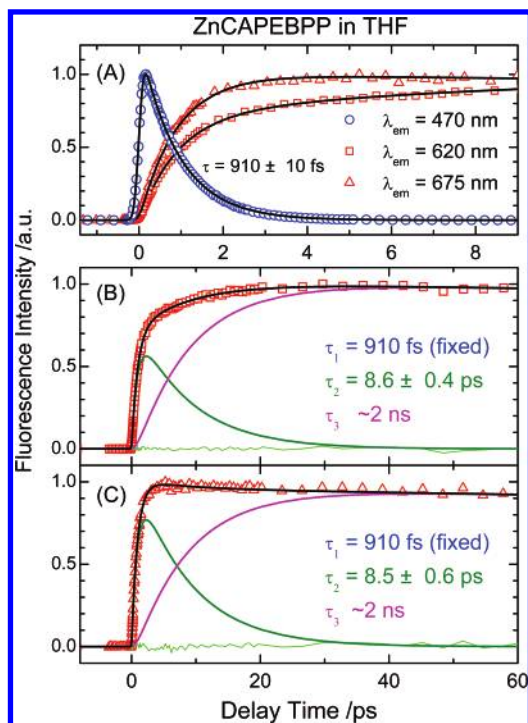
Figure 4. Femtosecond fluorescence transients of ZnCAPEBPP in THF solution (1×10^{-5} M) obtained at λ_{em}/nm = (A) 470 (open circles), (B) 620 (open squares), and (C) 675 (open triangles), with excitation at λ_{ex} = 420 nm for λ_{em} = 470 nm and λ_{ex} = 430 nm for λ_{em} = 620 and 675 nm. Open symbols denote raw data; solid black curves represent theoretical fits with residuals shown as green traces; the olive and magenta curves under each transient are deconvoluted components.

Figure 5. Femtosecond fluorescence transients of ZnCAPEBPP mixed with PMMA and spin-coated on a glass substrate obtained at λ_{ex} = 420 or 430 nm with fluorescence probed at λ_{em}/nm = (A) 460 (open circles), (B) 620 (open squares), and (C) 675 (open triangles). Excitation was performed at λ_{ex} = 420 nm for λ_{em} = 460 nm and λ_{ex} = 430 nm for λ_{em} = 620 and 680 nm. Open symbols denote raw data; solid black curves represent theoretical fits with residuals shown as green traces; the olive and magenta curves under each transient are deconvoluted components.

on the observed 100-ps scale ($\tau_3 \sim 2$ ns). As the transients observed at λ_{em} = 620 and 675 nm represent the relaxation dynamics of ZnCAPEBPP in the S_1 state, the observed two consecutive components might be assigned to the hot and cold S_1 species, respectively. Accordingly, the hot S_1 species were produced from the S_2 state in $\sim$1 ps. The excess vibrational energy in the hot S_1 species is released to the solvent molecules via vibrational relaxation, and this process yields the cold S_1 species being produced in $\sim$9 ps. The cold S_1 species are relatively enduring because $S_1 \rightarrow T_1$ intersystem crossing of ZnCAPEBPP in solution occurs in $\sim$2 ns, as is confirmed by our ps measurements. Our real-time observation on the Zn-CAPEBPP system is consistent with femtosecond results for the zinc tetraphenylporphyrin (ZnTPP) system, for which the lifetime of the S_2 state of ZnTPP is reported to be in a range 1.45−2.35 ps, and vibrational cooling from the nonrelaxed vibronic state of the hot S_1 species takes place on a time scale of $\sim$10 ps.[36−38]

3.3. Relaxation Dynamics of ZnCAPEBPP/PMMA Solid Films. When the ZnCAPEBPP molecules are evenly mixed with PMMA on a solid film, the observed fluorescence transients are similar to those in a homogeneous liquid solution. Figure 5A shows the corresponding transients of a ZnCAPEBPP/PMMA film with excitation performed at λ_{ex} = 420 nm and emissions observed at λ_{em} = 460, 620, and 680 nm. The transient at 460 nm was fitted with two components: the major part of the transient decays in 690 ± 20 fs but there exists a minor offset component that is persistent on a 10-ps scale. The transients observed at both 620 and 680 nm exhibit a rising feature that is comparable to the decay of the transient observed at 460 nm. According to the same fitting procedure employed for the solution data aforementioned, both transients were fitted according to a consecutive kinetic model with the corresponding

time coefficients τ_1, τ_2, and τ_3 evaluated to be 690 fs, 12 ps, and $\sim$2 ns, respectively. Our assignment for the observed excited-state dynamics of a ZnCAPEBPP/PMMA film is similar to the case in THF solution: the observed relaxation time $\tau_1 =$ 690 fs is due to efficient $S_2 \rightarrow S_1$ IC; the observed 12-ps component represents energy transfer from the hot S_1 species to the PMMA environment; the offset component ($\tau_3 \sim 2$ ns) is due to $S_1 \rightarrow T_1$ ISC from the cold S_1 species.

The observed relaxation period τ_1 = 690 fs in the transient of the ZnCAPEBPP/PMMA film is similar to that in THF solution (τ_1 = 910 fs). The former at λ_{em} = 460 nm involves, however, an "offset" component that is completely absent in the solution sample (Figure 5A vs Figure 4A), implying that some ZnCAPEBPP molecules in the PMMA film do not undergo $S_2 \rightarrow S_1$ IC to the S_1 state, probably due to the restriction of nuclear motions in the solid state. The observation of a dominating fast-decay component in the transient indicates that the $S_2 \rightarrow S_1$ IC is still a major process to be considered for ZnCAPEBPP isolated inside the PMMA matrix. Because large-amplitude nuclear motions of porphyrin molecules are restricted in the solid state whereas motions are relatively free in liquid solution, we expect that the observed offset signal in the former is due to the contribution of intramolecular motions constrained in the PMMA matrix that impedes the $S_2 \rightarrow S_1$ IC. We speculate that the in-plane expansion and compression motions of the porphyrin ring might be involved for such an efficient electronic relaxation to occur.

As mentioned earlier, the hot S_1 species were produced after IC from the S_2 state. In solution, the excess vibrational energy of ZnCAPEBPP in the S_1 state would be carried away in $\sim$9 ps by the solvent molecules (Figure 4B,C). For the PMMA film,
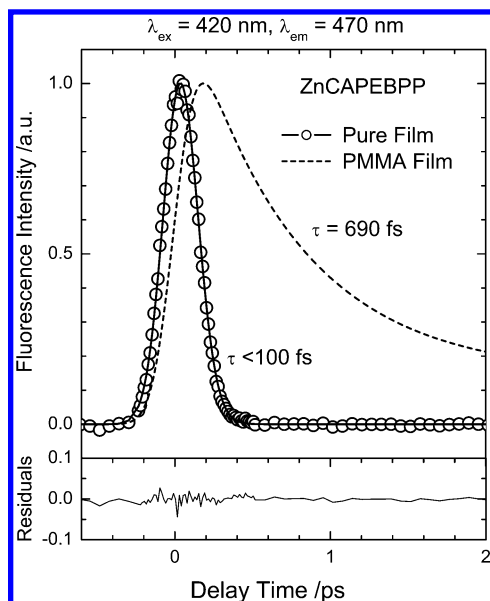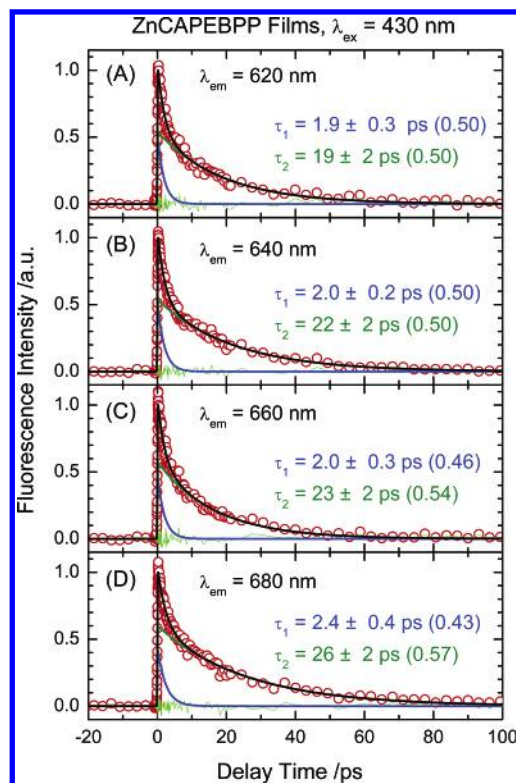
Figure 6. Femtosecond fluorescence transients of ZnCAPEBPP as a pure solid film on a glass substrate (open circles) obtained at $\lambda_{ex} =$ 420 nm with fluorescence probed at $\lambda_{em} =$ 470 nm (fwhm = 200 fs). The solid curve is the theoretical fit with residuals shown in the lower panel. The dashed curve shows a theoretical fit of the transient of a ZnCAPEBPP/PMMA film for comparison.

Figure 7. Femtosecond fluorescence transients of ZnCAPEBPP as a pure solid film on a glass substrate (open circles) obtained at $\lambda_{ex} =$ 430 nm with fluorescence probed at λ_{em}/nm = (A) 620, (B) 640, (C) 660, and (D) 680. Solid black curves represent theoretical fits with residuals shown as green traces; the blue and olive curves under each transient are deconvoluted components.

we observed that the vibrationally hot S_1 species transfer their excess internal energy into the surrounding PMMA in ~12 ps (Figure 5B,C). The similarity for the UV/visible spectra and the relaxation dynamics between the PMMA film and the solution sample indicates that the ZnCAPEBPP molecules were perfectly isolated inside the PMMA matrix in the solid state and that intermolecular interactions between porphyrin molecules become negligible.

3.4. Relaxation Dynamics of Pure ZnCAPEBPP Solid Films. When pure ZnCAPEBPP molecules were spin-coated as a thin film on a glass substrate without mixing with PMMA, two peculiar spectral features appear. First, the absorption bands of the sold film become broadened and the maxima are red-shifted as mentioned above (Figure 3). Second, the ZnCAPEBPP film shows no appreciable emission with use of a conventional spectrofluorometer, i.e., aggregation between porphyrins would produce strong intermolecular interactions, which would cause significant fluorescence quenching. Figure 6 shows the fluorescence transient of a ZnCAPEBPP film recorded at $\lambda_{ex} =$ 420 nm and $\lambda_{em} =$ 470 nm. The transient exhibits a spike-like temporal profile with the decay coefficient indeterminate because of limited time resolution of the instrument (τ <100 fs). That is, the $S_2 \rightarrow S_1$ IC process of ZnCAPEBPP becomes extremely rapid when the porphyrin molecules stack together to form aggregates on a plate-glass substrate and the hot S_1 species are produced within that time scale (<100 fs). To probe the S_1 dynamics of the ZnCAPEBPP thin film, the detection window must move to the longer wavelength region.

As our instrument cannot resolve the decay coefficient of the transient at $\lambda_{em} =$ 470 nm, we observed no rising character of transients taken at $\lambda_{em} =$ 620, 640, 660, and 680 nm, as shown from top to bottom in Figure 7, parts A−D, respectively. The transients shown in Figure 7 display a biexponential decay feature, which was fitted with two components: the rapid component decays in 1.9−2.4 ps whereas the slow component decays in 19−26 ps. The ns component was completely absent in all four transients. This evidence is important for us to rationalize quenching of fluorescence from porphyrins upon

aggregation. Because the intermolecular energy transfer between porphyrins is so rapid, the relatively slow $S_1 \rightarrow T_1$ ISC process is unlikely to compete, which causes the disappearance of the ns component in the transients and the quenching of the fluorescent intensity.

3.5. Relaxation Dynamics of ZnCAPEBPP on Nanocrystalline TiO$_2$ Films. We investigated the relaxation dynamics of ZnCAPEBPP/TiO$_2$ thin films to gain dynamical information for an understanding of the rate of interfacial electron transfer between porphyrin and a nanocrystalline semiconductor film. From results discussed in section 3.4, we understand that aggregation of porphyrins plays an important role in the observed relaxation dynamics. As a result, we prepared thin-film samples by controlling the initial immersion concentration of ZnCAPEBPP solutions to vary the adsorbed molecular density on three identical nanocrystalline TiO$_2$ films. Figure 8 shows absorption spectra of ZnCAPEBPP/TiO$_2$ thin-film samples from top to bottom with decreasing absorbance of the Q bands, i.e., ZnCAPEBPP is more concentrated on Film 3 but it is less condensed on Film 1. Note that the shapes and the positions of the Q bands shown in Figure 8 are very similar irrespective of their large discrepancies in optical density. This might indicate that there are no significant differences in the degree of aggregation for the samples with different optical densities, as was previously observed by Kamat and co-workers for cresyl violet dye adsorbed on metal oxide surfaces.[39] However, in our case the formation of H-aggregates of porphyrins on TiO$_2$ surfaces was very sensitive to the shape and position of the Soret band but it has very little influence for the Q bands (Figure 3). Therefore, the degree of aggregation might be different as the optical densities of ZnCAPEBPP on TiO$_2$ films were
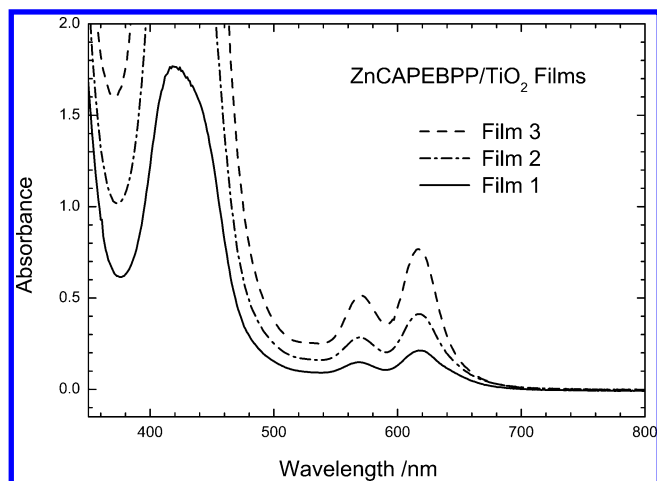
Figure 8. Absorption spectra of ZnCAPEBPP-sensitized TiO$_2$ films immersed in THF/CH$_2$Cl$_2$ (1:14) co-solvents at three concentrations of ZnCAPEBPP: 3.7×10^{-5} M (Film 1); 7.3×10^{-5} M (Film 2); and 1.5×10^{-4} M (Film 3). The immersion duration is 4 h for all three TiO$_2$ films.
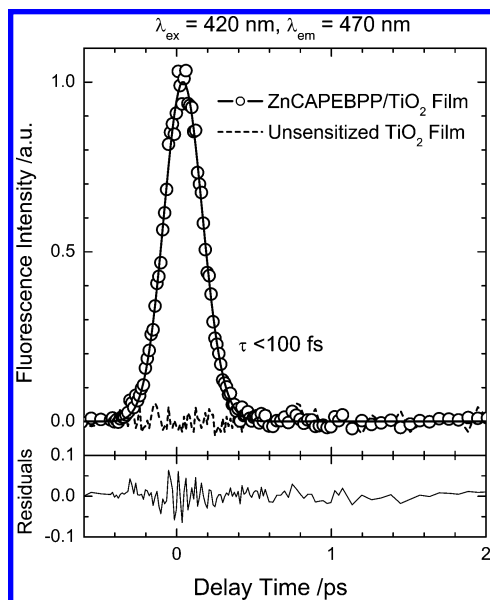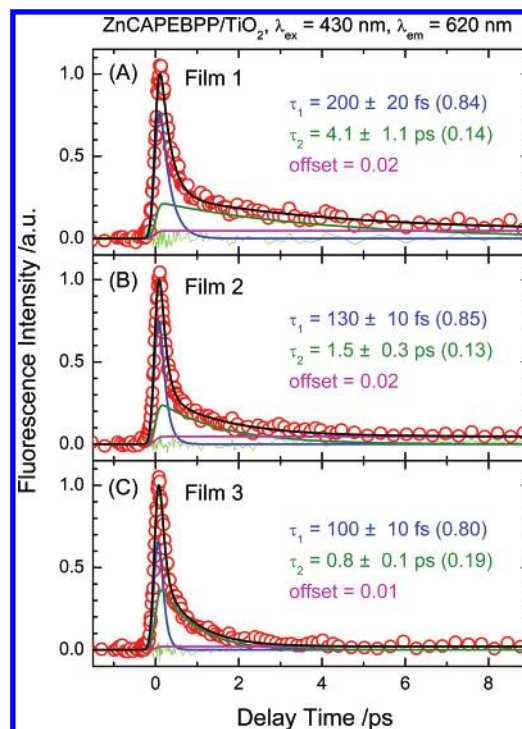

Figure 9. Femtosecond fluorescence transients of a ZnCAPEBPP-sensitized TiO$_2$ film (open circles) and an unsensitized TiO$_2$ film (dashed curves) obtained at λ_{ex} = 420 nm with fluorescence probed at λ_{em} = 470 nm (fwhm = 200 fs). The solid curve is the theoretical fit with residuals shown in the lower panel.

increased by a factor of 4; the corresponding dynamics will be discussed in the following.

Figure 9 shows the S$_2$ dynamics of a ZnCAPEBPP/TiO$_2$ film; the spike-like transient signal of the ZnCAPEBPP-sensitized TiO$_2$ film was observed at λ_{ex} = 420 nm and λ_{em} = 470 nm and no transient signal was observed for the unsensitized TiO$_2$ film (dashed curve shown in Figure 9). This dynamical feature is similar to that of ZnCAPEBPP thin-film samples that involved no TiO$_2$ nanoparticles: the observed ultrarapid relaxation dynamics ($<$100 fs) reflect not only the aggregate-induced energy transfer among porphyrins but also the interfacial electron transfer from porphyrin to TiO$_2$. The limited temporal resolution of our instrument precluded resolution of the IET dynamics from the transient.
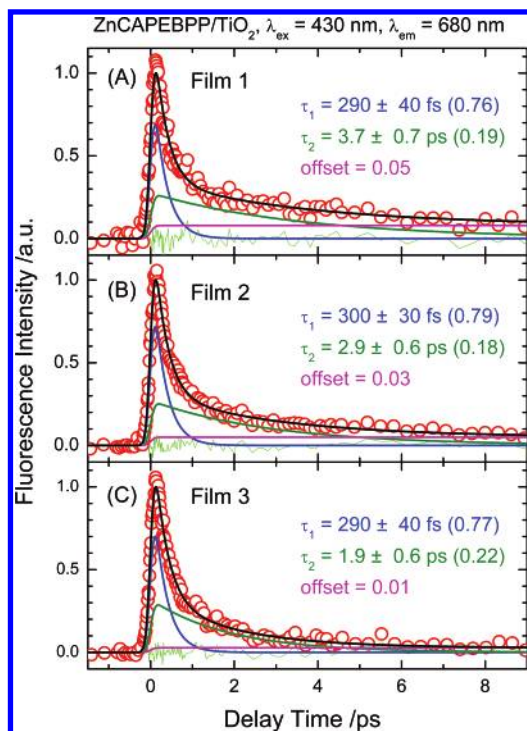
The relaxation dynamics of ZnCAPEBPP-sensitized TiO$_2$ films occurring in the S$_1$ state of porphyrin were studied with excitation at λ_{ex} = 430 nm and detection in the emission wavelength region 600−700 nm. Figure 10A−C displays in

Figure 10. Femtosecond fluorescence transients of ZnCAPEBPP-sensitized TiO$_2$ films under three conditions: (A) Film 1, (B) Film 2, and (C) Film 3, obtained at λ_{ex} = 430 nm with fluorescence probed at λ_{em} = 620 nm (fwhm = 220 fs). All transients are fitted with a parallel model with a small offset as indicated. Open circles denote raw data; solid black curves represent theoretical fits with residuals shown as green traces; the blue, olive and magenta curves under each transient are deconvoluted components.

three parts the fluorescence transients of Film 1−Film 3 at λ_{em} = 620 nm; Figure 11A−C shows the fluorescence transients of Film 1−Film 3 at λ_{em} = 680 nm. All transients were fitted with two decay components with a tiny offset. At λ_{em} = 620 nm, the rapid-decay coefficient τ_1 was observed to be 200 ± 20 fs in Film 1 but decreased to 130 ± 10 fs in Film 2 and further to 100 ± 10 fs in Film 3; the slow-decay coefficient τ_2 decreased significantly from 4.1 ± 1.1 ps in Film 1 to 0.8 ± 0.1 ps in Film 3; at λ_{em} = 680 nm, τ_1 is almost constant ($\sim$300 fs) for Film 1−Film 3 whereas τ_2 decreased from 3.7 ± 0.7 ps in Film 1 to 1.9 ± 0.6 ps in Film 3. The above real-time observations indicate three major points. First, due to the effect of aggregation, the S$_2 \rightarrow$ S$_1$ IC was still ultrarapid because we observed no rising character from all transients shown in Figures 10 and 11. Second, the values of τ_1 in the ZnCAPEBPP-sensitized TiO$_2$ films are less than one tenth those of Zn-CAPEBPP solid films (Figure 7), indicating that relaxation of the former is much more efficient than that of the latter; values of τ_2 in the former are comparable to the values of τ_1 in the latter. This comparison implies that one must consider the effect of aggregation of porphyrin to account for the observed slow relaxation dynamics of the former via intermolecular energy transfer.[26,33,40,41]

Third, although the slow relaxation coefficient τ_2 decreased significantly from the sample condition varying from small density (Film 1, OD = 0.2) to larger density (Film 3, OD = 0.8), the rapid decay periods are generally less sensitive (at λ_{em} = 620 nm) or insensitive (at λ_{em} = 680 nm) to the large variation of molecular density on the TiO$_2$ surface. The trend of variation of both τ_1 and τ_2 values at λ_{em} = 620 nm is consistent with involvement of an efficient energy transfer among isoenergetic porphyrin pigments: the fs component (τ_1) results from both

Femtosecond Fluorescence Dynamics of Porphyrin

J. Phys. Chem. B, Vol. 110, No. 1, 2006 **417**

Figure 11. Femtosecond fluorescence transients of ZnCAPEBPP-sensitized TiO$_2$ films under three conditions: (A) Film 1, (B) Film 2, and (C) Film 3, obtained at λ_{ex} = 430 nm with fluorescence probed at λ_{em} = 680 nm (fwhm = 220 fs). All transients are fitted with a parallel model with a small offset as indicated. Open circles denote raw data; solid black curves represent theoretical fits with residuals shown as green traces; the blue, olive and magenta curves under each transient are deconvoluted components.

forward IET and energy transfer at smaller intermolecular distance whereas the ps component (τ_2) arose mainly from energy transfer at a larger distance. At λ_{em} = 680 nm, resonance energy transfer in porphyrin aggregates is less efficient and occurs on a ps time scale to affect only the ps dynamics. The invariance of τ_1 values observed in all three sample conditions indicates that the fs component is due not to aggregation but to interfacial electron transfer between ZnCAPEBPP and TiO$_2$ nanostructure.[42]

Tachibana et al.[19] studied the electron-injection kinetics for a zinc porphyrin dye (ZnTCPP) sensitized on TiO$_2$ films using fs transient absorption; they found that adsorption of the porphyrin dye on TiO$_2$ films results in quenching of the stimulated emission that produces three relaxations on the time scales <100 fs, ~1 ps, and ~10 ps. As the optical density of a ZnTCPP-sensitized TiO$_2$ film (OD ~0.3) is similar to that of our low-density sample (OD ~0.2 in Film 1), the observed relaxation dynamics might be comparable. We seem to observe that electron injection from ZnCAPEBPP to TiO$_2$ at 680 nm is much slower than that from ZnTCPP to TiO$_2$: τ_1 ~290 fs (76%) vs <100 fs (37%); τ_2 ~4 ps (19%) vs ~1 ps (12%) and ~10 ps (51%). A small offset seems to be common to both cases. The amplitude of the fs component in our case is much larger than that of Tachibana et al., which might be due to the internal energy available from different excitations: the excitation of the former occurs in the S$_2$ state (λ_{ex} = 430 nm), whereas the excitation of the latter takes place in the S$_1$ state (λ_{ex} = 560 nm). We have shown that S$_2$ → S$_1$ electronic relaxation is ultrarapid, which would result in substantial amounts of hot S$_1$ species being produced in the former case. This condition is consistent with our results that the relaxation dynamics observed at 620 nm are much more rapid than those observed at 680 nm

because the detection window at the former wavelength would probe more "hot" species than that at the latter wavelength. We therefore conclude that the internal energy in the S$_1$ state of the former (ZnCAPEBPP) is much greater than that of the latter (ZnTCPP), which leads to an increased electron injection fraction (fs component) being observed for the former.

Moreover, we found that the molecular structure of the former is planar whereas that of the latter is nonplanar with the linker (phenyl group) twisted with respect to the porphine plane by ~60°. We thus expect that conjugation of the π-electrons in the former should be better than that in the latter. However, the IET rate of the former is slower than that of the latter; we think that this condition might reflect the number of anchoring carboxylate groups in porphyrin: there are four carboxylate groups in ZnTCPP but there is only one in ZnCAPEBPP. Hence, when ZnTCPP molecules are excited to the S$_1$ state, excited-state populations to a certain proportion (37%) undergo direct electron injection into the conducting band of TiO$_2$ within 100 fs; the other populations might be trapped in the excited state and undergo much slower relaxation via either indirect electron transfer or intermolecular energy transfer if aggregation is taken into account. For ZnCAPEBPP, there is only one-fourth the possibility for the S$_1$ species to undergo direct electron injection; hence this ultrarapid direct IET process (τ < 100 fs) is minor and unresolvable in our experiments. As a result, we assign the 300-fs relaxation period observed at 680 nm to be due to the majority of excited-state population (76%) undergoing *indirect* IET: the excited electrons in ZnCAPEBPP might be initially trapped in the porphine ring and seek an entrance to the electron-transfer bridge for indirect IET to occur. Because the phenyl-ethynyl group in ZnCAPEBPP is apparently better as an electron-transfer bridge than the phenyl group in ZnTCPP, we expect that searching for the entrance of the bridge is a bottleneck for the slower dynamics observed for the former. Therefore, to be consistent with the assignment of the dynamics, the observed ~300-fs relaxation period in the ZnCAPEBPP/ TiO$_2$ system might be compared with the ~1-ps relaxation period in the ZnTCPP/ TiO$_2$ system for the indirect IET process and the ~4-ps relaxation period of the former to be compared with the ~10-ps relaxation period of the latter for intermolecular energy transfer among porphyrins.

On the basis of the ultrarapid nature of the S$_2$ → S$_1$ IC observed for ZnCAPEBPP/TiO$_2$ films, we expect aggregation to be significant. Important dynamical evidence related to the aggregation that occurs in the S$_1$ state is discussed in the following. At λ_{em} = 620 nm (Figure 10), the relative amplitude of the ps component increases from 14% in Film 1 to 19% in Film 3; at λ_{em} = 680 nm (Figure 11), the relative amplitude of the ps component increases from 19% in Film 1 to 22% in Film 3. Moreover, the offset component becomes more pronounced in Film 1 than in Film 3. These observations indicate that the increased adsorption of porphyrin molecules on TiO$_2$ films enhances the contribution of the ps component. Hence both interfacial electron transfer and intermolecular energy transfer processes compete: when aggregation is less significant as in Film 1, the contribution of the fs component (due to the IET process) and the offset component (due to the monomer) would become more pronounced, and vice versa. Due to the red-shift spectral nature of aggregation in emission, we expect that the ps component would be more significant for transients observed at greater emission wavelengths; the relative amplitudes of the ps component observed at λ_{em} = 680 nm (Figure 11) are indeed larger than those observed at λ_{em} = 620 nm (Figure 10). Therefore, it supports the assignment of the observed slower

418 *J. Phys. Chem. B, Vol. 110, No. 1, 2006*

Luo et al.

ps-relaxation dynamics in ZnCAPEBPP-sensitized TiO$_2$ films being due mainly to intermolecular energy transfer via aggregation. The observed 1−4 ps aggregate-induced relaxation periods in ZnCAPEBPP-sensitized TiO$_2$ films are similar to those of the rapid relaxation in pure ZnCAPEBPP solid films (∼2 ps) but the slow-decay component (∼20 ps) of the latter is absent from the former. We think that this situation reflects aggregation of separate types: H-type aggregation is dominant in the former case whereas J-type aggregation prevails in the latter case.

4. Conclusion

Forward interfacial electron-transfer dynamics of a synthetic porphyrin sensitizer adsorbed on nanocrystalline TiO$_2$ films have been investigated by using femtosecond fluorescence up-conversion with S$_2$ excitation. The S$_2$ → S$_1$ electronic relaxation was found to be ultrarapid (<100 fs) because of aggregation of porphyrin molecules. The observed fluorescence transients in the S$_1$ state show a biphasic dynamical feature with two distinct time scales. Depending on the detection window, the rapid component decayed with τ_1 = 100−300 fs and the slow component with τ_2 = 0.8−4.1 ps. The fs component is assigned to indirect IET through a phenylethynyl bridge attached to one of four meso positions of the porphyrin ring. By means of a systematic variation of τ_2 as a function of molecular density on a TiO$_2$ surface, the ps component arose from intermolecular energy transfer among porphyrins. This evidence supports recent fs transient absorption results for ruthenium-complex-sensitized TiO$_2$ films in that the ps component was found to be due to the dye in an aggregated state.[18] The results obtained from time-resolved investigations of porphyrin in solution, directly deposited on solid films, and mixed with PMMA on solid films have also demonstrated the significance of aggregation affecting the observed relaxation dynamics in the solid phase.

References and Notes

(1) (a) Hagfeldt, A.; Grätzel, M. *Chem. Rev.* **1995**, *95*, 49−68. (b) Hagfeldt, A.; Grätzel, M. *Acc. Chem. Res.* **2000**, *33*, 269−277.

(2) Kalyanasundaram, K.; Grätzel, M. *Coord. Chem. Rev.* **1998**, *77*, 374−414.

(3) Grätzel, M.; *Nature* **2001**, *414*, 338−344.

(4) Tachibana, Y.; Moser, J. E.; Grätzel, M.; Klug, D. R.; Durrant, J. R. *J. Phys. Chem.* **1996**, *100*, 20056−20062.

(5) (a) Asbury, J. B.; Ellingson, R. J.; Ghosh, H. N.; Ferrere, S.; Nozik, A. J.; Lian, T. *J. Phys. Chem. B* **1999**, *103*, 3110−3119. (b) Wang, Y.; Asbury, J. B.; Lian, T. *J. Phys. Chem. A* **2000**, *104*, 4291−4299. (c) Asbury, J. B.; Hao, E.; Wang, Y.; Lian, T *J. Phys. Chem. B* **2000**, *104*, 11957-11964. (d) Asbury, J. B.; Hao, E.; Wang, Y.; Ghosh, H. N.; Hirendra, N. G.; Lian, T. *J. Phys. Chem. B* **2001**, *105*, 4545−4557. (e) Asbury, J. B.; Anderson N. A.; Hao, E.; Ai, X.; Lian, T *J. Phys. Chem. B* **2003**, *107*, 7376−7386.

(6) (a) Anderson N. A.; Ai, X.; Lian, T *J. Phys. Chem. B* **2003**, *107*, 14414−14421. (b) Ai, X.; Guo, J.; Anderson N. A.; Lian, T *J. Phys. Chem. B* **2004**, *108*, 12795−12803.

(7) (a) Benkö, G.; Kallioninen, J.; Korppi-Tommola, J. E. I.; Yartsev, A. P.; Sundström, V. *J. Am. Chem. Soc.* **2002**, *124*, 489−493. (b) Kallioninen, J.; Benkö, G.; Sundström, V.; Korppi-Tommola, J. E. I.; Yartsev, A. P. *J. Phys. Chem. B* **2002**, *106*, 4396−4404. (c) Pan, J.; Benkö, G.; Xu, Y.; Poscher, T.; Sun, L.; Sundström, V.; Polívka, T. *J. Am. Chem. Soc.* **2002**, *124*, 13949-13957. (d) Benkö, G.; Myllyperkiö, Pan, J.; Yartsev, A. P.; Sundström, V. *J. Am. Chem. Soc.* **2003**, *125*, 1118−1119. (e) Benkö, G.; Kallioninen, J.; Myllyperkiö, P.; Trif, F.; Korppi-Tommola, J. E. I.; Yartsev, A. P.; Sundström, V. *J. Phys. Chem. B* **2004**, *108*, 2862−2867. (f) Kallioninen, J.; Benkö, G.; Myllyperkiö, P.; Khriachtchev, L.; Skärman, B.; Wallenberg, R.; Tuomikoski, M.; Korppi-Tommola, J.; Sundström, V.; Yartsev, A. P. *J. Phys. Chem. B* **2004**, *108*, 6365−6373. (g) Pan, J.; Xu, Y.; Sun, L.; Sundström, V.; Polívka, T. *J. Am. Chem. Soc.* **2004**, *126*, 3066−3067. (h) Pan, J.; Xu, Y.; Benkö, G.; Feyziyev, Y.; Styring, S.; Sun, L.; Akermark, B.; Yartsev, A. P.; Sundström, V. *J. Phys. Chem. B* **2004**, *108*, 12904−12910.

(8) Kuciauskas, D.; Monat, J. E.; Villahermosa, R.; Gray, H. B.; Lewis, N. S.; McCusker, J. K. *J. Phys. Chem. B* **2002**, *106*, 9347−9358.

(9) Rehm, J. M.; McLendon, G. L.; Nagasawa, Y.; Yoshihara, K.; Moser, J.; Grätzel, M. *J. Phys. Chem.* **1996**, *100*, 9577−9578.

(10) Cherepy, N. J.; Smestad, G. P.; Grätzel, M.; Zhang, J. Z. *J. Phys. Chem. B* **1997**, *101*, 9342−9351.

(11) Martini, I.; Hodak, J. H.; Hartland, G. V. *J. Phys. Chem. B* **1998**, *102*, 9508−9517.

(12) Hilgendorff, M.; Sundström, V. *J. Phys. Chem. B* **1998**, *102*, 10505−10514.

(13) Huber, R.; Moser, J.-E.; Grätzel, M.; Wachtveitl, J. *J. Phys. Chem. B* **2002**, *106*, 6494−6499.

(14) Pelet, S.; Grätzel, M.; Moser, J.-E. *J. Phys. Chem. B* **2003**, *107*, 3215−3224.

(15) Biju, V.; Micic, M.; Hu, D.; Lu, H. P. *J. Am. Chem. Soc.* **2004**, *126*, 9374−9381.

(16) Ramakrishna, G.; Singh A. K.; Palit, D. K.; Ghosh, H. N. *J. Phys. Chem. B* **2004**, *108*, 4775−4783.

(17) Xiang, J.; Rondonuwu, F. S.; Kakitani, Y.; Fujii, R.; Watanabe, Y.; Koyama, Y.; Nagae, H.; Yamano, Y.; Ito, M. *J. Phys. Chem. B* **2005**, *109*, 17066−17077.

(18) Wenger, B.; Grätzel, M.; Moser, J.-E. *J. Am. Chem. Soc.* **2005**, *127*, 12150−12151.

(19) Tachibana, Y.; Haque, S. A.; Mercer, I. P.; Durrant, J. T.; Klug, D. R. *J. Phys. Chem. B* **2000**, *104*, 1198−1205.

(20) Kalyanasundaram, K.; Vlachopoulos, N.; Krishnan, V.; Monnier, A.; Grätzel, M. *J. Phys. Chem.* **1987**, *91*, 2342−2347.

(21) Koehorst, R. B. M.; Boschloo, G. K.; Savenije, T. J.; Goossens, A.; Schaafsma, T. J. *J. Phys. Chem. B* **2000**, *104*, 2371−2377.

(22) Cherian, S.; Wamser, C. C. *J. Phys. Chem. B* **2000**, *104*, 3624−3629.

(23) Viseu, T. M. R.; Hungerford, G.; Ferreira, M. I. C. *J. Phys. Chem. B* **2002**, *106*, 1853−1861.

(24) Noguera, A. F.; Furtado, L. F. O.; Nakamura, M.; Araki, K.; Toma, H. E. *Inorg. Chem.* **2004**, *43*, 396−398.

(25) Balzani, L.; Credi, A.; Venturi, M. *Molecular Devices and Machines*; Wiley-VCH: Weinheim, Germany, 2003; and related references therein.

(26) (a) Kim, D.; Osuka, A.*J. Phys. Chem. A* **2003**, *107*, 8791−8816. (b) Kim, D.; Osuka, A. *Acc. Chem. Res.* **2004**, *37*, 735−745. (c) Hwang, I.-W.; Aratani, N.; Osuka, A.; Kim, D *Bull Korean Chem. Soc.* **2005**, *26*, 1−13.

(27) Hasobe, T.; Kamat, P. V.; Troiani, V.; Solladié, N.; Ahn, T. K.; Kim, S. K.; Kim, D.; Kongkanand, A.; Kuwabata, S.; Fukuzumi, S. *J. Phys. Chem. B* **2005**, *109*, 19−23.

(28) Holten, D.; Bocian, D. F.; Lindsey, J. S. *Acc. Chem. Res.* **2002**, *35*, 57−69.

(29) (a) Sonogashira, K.; Tohda, Y.; Hagihara, N. *Tetrahedron Lett.* **1975**, 4467−4470. (b) Takahashi, S.; Kuroyama, Y.; Sonogashira, K. *Synthesis* **1980**, 627−630.

(30) Perrin, D. D.; Armarego, W. L. F. *Purification of laboratory chemicals*, 3rd ed.; Pergamon Press: Oxford, UK, 1988.

(31) Barbe, C. J.; Arendse, F.; Comte, P.; Jirousek, M.; Lenzmann, F.; Shklover, V.; Grätzel, M. *J. Am. Ceram. Soc.* **1997**, *80*, 3157.

(32) (a) Lu, Y.-C.; Chang, C.-W.; Diau, E. W.-G. *J. Chin. Chem. Soc.* **2002**, *49*, 693−701. (b) Lu, Y. C.; Diau, E. W.-G.; Rau, H. *J. Phys. Chem. A* **2005**, *109*, 2090−2099.

(33) Valeur, B. *Molecular Fluorescence;* Wiley-VCH: Weinheim, Germany, 2002; Chapter 6, and other related references therein.

(34) Pedersen S.; Zewail, A. H. *Mol. Phys.* **1996**, *89*, 1455−1502.

(35) (a) Campbell, W. M.; Burrell, A. K.; Officer, D. L.; Jolley, K. W. *Coord. Chem. Rev.* 2004, *248*, 1363−1379. (b) Nappa, M.; Valentine, J. S. *J. Am. Chem. Soc.* **1978**, *100*, 5075−5080.

(36) Gurzadyan, G. G.; Tran-Thi, T.-H.; Gustavsson, T. *J. Chem. Phys.* **1998**, *108*, 385−388.

(37) Mataga, N.; Shibata, Y.; Chosrowjan, H.; Yoshida, N.; Osuka, A. *J. Phys. Chem. B* **2000**, *104*, 4001−4004.

(38) Yu, H.; Baskin, J. S.; Zewail, A. H. *J. Phys. Chem. A* **2002**, *106*, 9845−9854.

(39) (a) Liu, D.; Kamat, P. V. *J. Chem. Phys.* **1996**, *105*, 965−970. (b) Martini, I.; Hartland, G. V.; Kamat, P. V. *J. Phys. Chem. B* **1997**, *101*, 4826−4830.

(40) Rubtsov, I. V.; Kobuke, Y.; Miyaji, H.; Yoshihara, K. *Chem. Phys. Lett.* **1999**, *308*, 323−328.

Femtosecond Fluorescence Dynamics of Porphyrin

J. Phys. Chem. B, Vol. 110, No. 1, 2006 **419**

(41) Larsen, J.; Andersson, J.; Polívka, T.; Sly, J.; Crossley, M. J.; Sondström, V.; Akesson, E. K. *Chem. Phys. Lett.* **2005**, *403*, 205–210.

(42) The observed discrepancies in the relaxation dynamics might arise from the differences in the state of aggregation of the dye, i.e., the femtosecond components shown in Figures 10 and 11 are due to H-aggregation of ZnCAPEBPP on TiO$_2$ films while this dynamical feature is absent as the dye forming J-aggregates on glass plate (Figure 7). However, previous study on J- and H-aggregates of porphyrin-surfactant complexes (*J. Phys. Chem. B* **1998**, *102*, 1528) indicates that the fluorescence decay of the H-aggregate (1.1 and 8.9 ns) is much slower than that of the J-aggregate (∼0.1 ns), which supports our assignment for the femtosecond component being due to interfacial electron transfer between porphyrin and TiO$_2$.